

An Ising Hamiltonian Solver using Stochastic Phase-Transition Nano-Oscillators

S. Dutta^{1†}, A. Khanna^{1†}, H. Paik³, D. Schlom³, A. Raychowdhury⁴,
Z. Toroczkai² and S. Datta^{1*}

¹Department of Electrical Engineering, University of Notre Dame, Notre Dame, IN 46556, USA

²Department of Physics, University of Notre Dame, Notre Dame, IN 46556, USA

³Department of Materials Science and Engineering, Cornell University, Ithaca, NY 14853, USA

⁴School of Electrical and Computer Engineering, Georgia Institute of Technology, Atlanta, GA
USA

[†]These authors contributed equally to this work

*Corresponding author email: sdatta@nd.edu

Computationally hard problems, including combinatorial optimization, can be mapped into the problem of finding the ground-state of an Ising Hamiltonian. Building physical systems with collective computational ability and distributed parallel processing capability can accelerate the ground-state search. Here, we present a continuous-time dynamical system (CTDS) approach where the ground-state solution appears as stable points or attractor states of the CTDS. We harness the emergent dynamics of a network of phase-transition nano-oscillators (PTNO) to build an Ising Hamiltonian solver. The hardware fabric comprises of electrically coupled injection-locked stochastic PTNOs with bi-stable phases emulating artificial Ising spins. We demonstrate the ability of the stochastic PTNO-CTDS to progressively find more optimal solution by increasing the strength of the injection-locking signal – akin to performing classical annealing. We demonstrate in silico that the PTNO-CTDS prototype solves a benchmark non-deterministic polynomial time (NP)-hard Max-Cut problem with high probability of success. Using experimentally calibrated numerical simulations, we investigate the performance of the hardware with increasing problem size. We show the best-in-class energy-efficiency of 3.26×10^7 solutions/sec/Watt which translates to over five orders of magnitude improvement when compared with digital CMOS, quantum and photonic Ising solver approaches. We also demonstrate an order of magnitude improvement over a discrete-time memristor-based Hopfield network approach. Such an energy efficient CTDS hardware exhibiting high solution-throughput/Watt can find application in industrial planning and manufacturing, defense and cyber-security, bioinformatics and drug discovery.

Combinatorial optimization is ubiquitous in various fields such as artificial intelligence, bioinformatics, drug discovery, cryptography, quantitative finance, operations research, resource allocation, trajectory and route planning. Such problems belong to the NP-hard or NP-complete complexity class, requiring computational resources (time and/or energy) that scale exponentially with the problem size. Interestingly, many combinatorial optimization problems can be translated into another fundamental physics problem of finding the ground state of an Ising model (1) (or its equivalent Quadratic Unconstrained Binary Optimization (QUBO) problem (2)). The Ising model, describing the property of spin glass, was put forward as a tool of statistical physics to explain the phenomenon of ferromagnetism. The Ising Hamiltonian with N discrete spins $\sigma_{1 \leq i \leq N} \in \{-1, +1\}^N$

and a symmetric coupling matrix J in the absence of an external magnetic field is given by $H = -\sum_{i=1}^N J_{ij} \sigma_i \sigma_j$.

Finding the ground state of Ising model belongs to the NP-hard complexity class (3) and can be extended to other NP-hard and NP-complete problems including all of Karp's twenty-one NP-complete problems through polynomial time mapping (4). Solving the Ising model using exact methods such as the branch-and-bound algorithm are often limited to problem sizes of only a few hundred variables. Alternatively, approximate algorithms or heuristics and stochastic approaches such as semidefinite program (5), breakout local search (6), metropolis algorithm (7) and simulated annealing (8) are widely used in digital computers to find an optimal or near-optimal solution. Even for moderately sized problem instances, the time to find a near-optimal solution can become prohibitively large. Hence, there is a growing interest towards finding hardware approaches, beyond digital CMOS, that can solve large-scale constrained optimization problems efficiently. Recently, various schemes for building annealing-inspired non-von Neumann processors, called Ising machines, have been devised on a variety of technology platforms. These include superconducting qubit-based adiabatic quantum computing (AQC) and quantum annealing (9, 10), digital and mixed-signal complementary metal-oxide-semiconductor (CMOS) annealers (11–13) and coherent networks of degenerate optical parametric oscillators (14, 15). Qubit-based quantum annealers incur high cost and complexity arising from operation in cryogenic environment. The optical coherent Ising machine has shown competitive performance compared to the quantum annealer (16), but requires kilometer long fiber ring cavity for implementing 2,000 spins using temporal multiplexing and require extremely fast (and power hungry) field-programmable gate array (FPGA) for implementing coupling in a measure-and-feedback scheme (15). Digital CMOS annealers (11–13) rely on an external source for random number generation for introducing stochasticity and find it technologically challenging to maintain true randomness in CMOS implementation, while requiring significant post-processing.

One alternative pathway is to utilize a continuous-time dynamical system (CTDS) approach. Dynamical systems are defined by the change in the state of the system (say $x(t)$) with respect to time (t). In particular, a continuous-time dynamical system can be described by the time evolution of state, $x(t)$, as $\frac{dx(t)}{dt} = f(x)$, where f is a linear or non-linear function describing the change in the dependence of the state. Recently, a vast repertoire of emergent dynamics exhibited by CTDS has been exploited across a wide range of fields from understanding the neural activity in the human brain (17, 18) to synchronized locomotion control (19, 20). Using a CTDS approach, it is possible to solve a combinatorial optimization problem that involves setting up the system appropriately such the stable point or the attractor state represents the solution of the problem. As the system evolves in time, it can dynamically find the global minima through energy minimization. Because of the inherent distributed nature and parallel processing capability, dynamical systems can find the ground state or near-optimum solution with immense speed-up compared to a sequentially working digital computer. In this work, we report an electronic phase-transition nano-oscillator (PTNO)-based CTDS that acts as an Ising Hamiltonian solver. The optimization problem, i.e. the Ising energy to be minimized is encoded as the inherent “energy” or Lyapunov function of the PTNO-CTDS. Through emergent synchronized dynamics, the PTNO-CTDS performs collective computing and rapidly attempts to find the global minima. Additionally, the PTNOs operate at room temperature and consume extremely low power which translates to several orders of magnitude improvement in energy-efficiency (solution-throughput/Watt) when

compared with digital CMOS, quantum and photonic approaches and a discrete-time memristor-based Hopfield network approach (21).

Overview of PTNO-based CTDS as an Ising Hamiltonian solver

The combinatorial optimization problem is reformulated in terms of the Ising Hamiltonian H defined by the spin vector $\vec{\sigma}$, and the symmetric coupling matrix J and mapped onto the Ising solver as shown in Fig. 1(a) and (b). Each Ising spin, representing a node in the graph is emulated by an insulator-to-metal phase-transition (IMT) nano-oscillator. A PTNO comprises a two-terminal phase-transition hysteretic device in series with a transistor as shown in Fig. 1(c). We use Vanadium Dioxide (VO_2) as a prototypical IMT material in our experiments (22). A false-colored SEM image of a two-terminal VO_2 of length = $1\mu\text{m}$ used in our experiments is shown in Fig. 1(c). The working principle of VO_2 -based PTNO has been reported earlier elsewhere (19, 23, 24). Below the phase-transition temperature and under zero external electric field or current, VO_2 shows insulating behavior. Upon application of an electric field across the two terminals of the device that forces current to flow through, the material undergoes an abrupt phase transition from insulating to metallic state. The hysteretic phase transition is reflected as an abrupt hysteretic current-voltage (I-V) characteristic of the device. Pairing a conventional n-type metal-oxide-semiconductor (NMOS) transistor in series with the VO_2 such that the load line passes through the unstable region of the I-V curve results in self-sustained oscillations as show in fig. 1(c). We used $V_{\text{DD}} = 2\text{V}$ and a gate voltage $V_{\text{GS}} = 0.9\text{V}$ in our experiments. We create a highly interconnected PTNO-network where the coupling matrix W is derived from the adjacency or coupling matrix J of the Ising model as shown in Fig. 1(a) and (b). In this example of Ising model with antiferromagnetic interactions, the presence of an edge between two nodes is denoted as $J = -1$ and is represented by a coupling capacitance C_C .

Fig.1(d) shows an overview of the experimental setup of the PTNO-based CTDS. The main computing kernel comprises eight PTNOs connected using coupling capacitance following the coupling matrix W . The fabricated VO_2 device array (labeled as 1-8 in Fig. 1(d)) are connected with eight NMOS transistors in series to create eight PTNOs. To emulate artificial Ising spins $\vec{\sigma}$, an external injection locking signal S_{INJ} is applied to all the oscillators using injection capacitances C_{INJ} . As explained later, this creates bi-stable oscillator phases $\vec{\theta}$ that are used as state variables for computing. The continuous-time dynamics of the network is dictated by an “energy” or the Lyapunov function $E(\vec{\theta})$ that closely resembles the Ising Hamiltonian H . The dynamics of the network evolves continuously in time, so as to naturally minimize $E(\vec{\theta})$, and in the process minimizes the Ising Hamiltonian to reach the ground state as shown in Fig. 1(e). Once the network reaches an energy minima state, the output of the network is read out in terms of the state variables $\vec{\theta}$ and subsequently reformulated to provide the optimal solution of the original optimization problem. One formidable challenge in solving combinatorial optimization problem is the inevitable increase in the complexity of the energy landscape with the problem size. Specifically, the presence of a large number of local minima degrades the probability of reaching a global optimum. Stochasticity is a well-known technique utilized in Boltzmann machines and simulated annealing, to overcome the issue of getting trapped in local minima. In the latter case, a stochastic noise is used to perturb the state of the system and the magnitude of noise is reduced slowly over time (replicated as a change in the temperature parameter in the algorithm) as the system approaches the global optimum. In our system, we exploit the inherent stochasticity present in the

IMT material (25) to escape the local minima as well as introduce a novel way of gradually reducing the temporal fluctuations in the oscillator phases by increasing the strength of the injection locking signal S_{INJ} . This allows us to perform classical annealing operation and obtain progressively better solutions as illustrated schematically in Fig. 1(e).

Artificial Ising spin

The binary degrees of freedom in the phase space of PTNOs arises from the phenomenon of second harmonic injection locking. We apply a sinusoidal injection locking signal $S_{inj} = V_{inj} \sin(2\pi f_{inj} t)$ with $f_{inj} = 2f_0$ as an external input to the oscillators across the capacitor $C_{inj} = 20 \text{ pF}$ as shown in Fig. 1(d). When $V_{inj} = 0$, the oscillator is free running. Fig. 2(a, i) shows the voltage output waveform V_{out} measured over multiple runs. The corresponding phase of the oscillator, measured with respect to a reference sinusoidal signal of same frequency f_0 , shows a constantly varying phase with a uniform probability distribution over the entire phase space as seen Fig. 2(b, i). In contrast, when the oscillator is perturbed with S_{inj} at the first harmonic, i.e. $f_{inj} \approx f_0$ also referred to as first harmonic injection locking (FHIL), V_{out} shows a constant 80° phase locking configuration with S_{inj} as seen in Fig. 2(a, ii). The probability distribution of the phase, measured over multiple runs, shows a single gaussian distribution as shown in Fig. 2(b, ii). Interestingly, when $f_{inj} \approx 2f_0$, the oscillator waveform shows both in-phase (40°) and out-of-phase (220°) injection locking configuration when measured over multiple runs as seen in Fig. 2(a, iii). The corresponding probability distribution shown in Fig. 2(b, iii) exhibits a double gaussian distribution highlighting an equiprobable and bi-stable phase portrait. This bi-stability provides an ideal means to encode the Ising spin in the electrical domain, where phase 40° represents up-spin, i.e., $= +1$, and phase 220° represents down-spin, i.e., $\sigma = -1$.

The continuous-time dynamics of the phase difference θ between the oscillator and the injection locking signal can be described by a generalized version of Adler's equation (Gen-Adler) given by

$$\frac{d\theta(t)}{dt} = -(f_{inj} - n_H f_0) + K_{inj}^H \int_0^{2\pi} \xi(\theta(t) + \vartheta) \cos(\vartheta) d\vartheta \quad (1)$$

where n_H is the n^{th} harmonic of the IMT nano-oscillator and $K_{inj}^H = 2\pi n_H f_0 f_{inj} C_{inj} V_{inj}$. The first term describes the frequency mismatch between V_{out} and S_{inj} , which contributes to *phase slipping*. The second term depends on the phase delay incurred due to the perturbation caused by S_{inj} and is described in terms of the perturbation-projection-vector (PPV), ξ (see Supplementary information section S1 and S2 for details). The corresponding "energy" function or Lyapunov function of the oscillator is given by

$$E(\theta) = (f_{inj} - n_H f_0)\theta - K_{inj}^H \int_0^\theta \int_0^{2\pi} \xi(\phi + \vartheta) \cos(\vartheta) d\vartheta d\phi \quad (2)$$

The first energy term comes from the contribution of the frequency mismatch that creates an overall bias in the energy landscape. However, this being a linear term does not introduce any additional valleys or peaks in the energy landscape. The second term describes the interaction between the injection locking signal and the oscillator. The corresponding probability distribution of the oscillator's phase can be calculated as $P(\theta_i) = \frac{e^{-E(\theta_i)/\eta}}{Z}$, where $Z = \sum_i e^{-E(\theta_i)/\eta}$ is the

partition function and η is analogous to the kT term in the Boltzmann distribution and can be interpreted as a measure of the stochastic noise in the IMT oscillator. Expectedly, with zero injection locking, the “energy” function of the oscillator stays flat as shown in Fig. 2(b) indicating a uniform distribution over the phase space as is experimentally obtained in Fig. 2(a). For first harmonic injection locking (FHIL), as long as the relative frequency difference ($f_{inj} - f_o$) is small compared to the second term in equation, $\frac{d\theta(t)}{dt} = 0$ exhibits one stable point at $\theta \cong 0.4\pi$, i.e. one injection-locked equilibrium phase and the calculated $E(\theta)$ (assuming zero frequency mismatch) displays a single energy minima. This results in a single gaussian peak in the probability distribution of the oscillator’s phase as verified experimentally. In the case of SHIL, $\frac{d\theta(t)}{dt}$ exhibits two stable points at $\theta \cong 0.2\pi$ and $\theta \cong 1.2\pi$, i.e. two equilibrium phases. The calculated $E(\theta)$ (assuming zero frequency mismatch) evolves into a double well energy landscape that results in a double gaussian distribution in the phase space as reproduced faithfully in the measurements (see Supplementary information section S1 and S2 for further details).

The steady-state analysis of the Gen-Adler equation in the case of SHIL also predicts that, in the presence of a frequency mismatch between the oscillator and the injection locking signal, there exists a critical amplitude of the injection signal V_{inj} below which no stable solution exists. In our experiments, this critical amplitude is close to 1V for a frequency mismatch of 3% as observed in the measurements. Above this threshold, the bi-stability in the phase space begins to appear. Fig. 2(c) shows the measured oscillator phase as a function of the amplitude of the injection signal, V_{inj} . For very low V_{inj} close to the critical value, the phase of the oscillator measured over multiple runs shows a wide distribution in the phase space, with the distribution narrowing as V_{inj} increases. This behavior can be understood by considering the perturbation in the energy landscape as shown in Fig. 2(e) for $V_{inj} = 1V, 3V$ and $5V$. For $V_{inj} = 1V$, the energy barrier E_B separating the two stable equilibrium phases is low (around $E_B = 0.006$ calculated from Eq. 3). Hence, in the presence of stochastic noise, the oscillator’s phase constantly fluctuates between the two stable phases as seen in the Fig. 2(d). An increase in V_{inj} to 3V and 5V increases the barrier height E_B to 0.012 and 0.02, respectively. This reduces the fluctuations in the measured oscillator’s phase. This is reflected in the experimentally measured mean time between each phase flip, referred to as the dwell time τ_{Dwell} (analogous to *Neel relaxation time* for magnetization) as a function of V_{inj} as shown in Fig. 2(f). The increase in τ_{Dwell} with increasing V_{inj} accurately follows the Arrhenius’s relation $\tau_{Dwell} = \alpha\tau_0 e^{\frac{E_B}{\eta}}$, where $\tau_0 = \frac{1}{f_0}$ is the characteristic or attempt time (equal to the time period of the oscillator), α is the fitting parameter and η is the stochastic noise in the IMT oscillator. This characteristic of reduction in the temporal fluctuations of the oscillator’s phase with increasing amplitude of injection locking signal proves to be key knob towards performing classical annealing in our hardware.

Replicating the interaction term in the Ising Hamiltonian

To implement an asynchronous PTNO-CTDS that can replicate an artificial Ising spin system, the oscillators need to be connected to one another using coupling elements that emulate the ferromagnetic and antiferromagnetic nature of interaction. We first study the nature of interaction in a pairwise coupled oscillator system as shown schematically in Fig. 3(a) using capacitance C_C as the coupling element. Fig. 3(b) shows the experimentally measured phase distribution of the

two oscillators using an injection locking capacitance $C_{inj} = 20 \text{ pF}$ and coupling capacitance $C_C = 56 \text{ pF}$. The oscillators remain out-of-phase with each other and the two configurations: $(40^\circ, 220^\circ)$ and $(220^\circ, 40^\circ)$ are two equally probable states. We measured the probability of out-of-phase configuration for varying coupling strength as shown in Fig. 3(c). The probability remains close to 0.5 for low coupling capacitance, meaning both in-phase and out-of-phase configurations are equally probable, and increases close to 1 for stronger coupling. We also compare our experimental results with experimentally calibrated PPV-based numerical simulations (methodology described in the Materials and Methods section later) as shown in Fig. 3(c) showing excellent agreement. To understand the exact nature of capacitive coupling, we compare it with a 2-spin Ising model with antiferromagnetic interaction (negative J) where the individual spins prefer to remain anti-parallel with one another. In such a system, the probability of one of the possible configurations- $(\uparrow\uparrow, \downarrow\downarrow, \uparrow\downarrow, \downarrow\uparrow)$ is determined by the Boltzmann distribution $P(\sigma_1, \sigma_2) = e^{-H(\sigma_1, \sigma_2)/kT}/Z$, where T is temperature and $Z = \sum_{\sigma_1, \sigma_2} e^{-H(\sigma_1, \sigma_2)/kT}$ is the partition function. With antiferromagnetic interaction (negative J), the probability for anti-parallel configuration $(\uparrow\downarrow, \downarrow\uparrow)$ increases upon varying the interaction strength from $J = 0$ to -2 . Thus, the antiferromagnetic interaction in an Ising Hamiltonian can be faithfully replicated using capacitive coupling in this IMT nano-oscillator-based system.

Mathematically, the continuous-time dynamics of such a PTNO network can be further described by extending Eq. 2 and Eq. 3 to incorporate an additional coupling term and is given by

$$\begin{aligned} \frac{d\theta_i(t)}{dt} = & -(f_{inj} - n_H f_{o,i}) + K_{inj,i}^H \int_0^{2\pi} \xi_i(\theta_i(t) + \vartheta) \cos(\vartheta) d\vartheta \\ & + f_0 \sum_{j=1, j \neq i}^N \int_0^{2\pi} \xi_i(\theta(t) + \vartheta) I_{osc,j} d\vartheta \end{aligned} \quad (3)$$

where $I_{osc,j} = C_{C,j} \frac{dV_{osc,j}}{dt}$. The additional third term describes the coupling interaction energy between pairs of oscillators. The corresponding “total energy” function or the global Lyapunov function of the PTNO-CTDS is then given by

$$\begin{aligned} E(\vec{\theta}) = & \sum_{i=1}^N (f_{inj} - n_H f_0) \theta_i - K_{inj}^H \sum_{i=1}^N \int_0^{\theta_i} \int_0^{2\pi} \xi_i(\phi + \vartheta) \cos(\vartheta) d\vartheta d\phi \\ & - f_0 \sum_{i,j=1, i \neq j}^N \int_0^{\theta_i} \int_0^{2\pi} \xi_i(\phi + \vartheta) I_{osc,j} d\vartheta d\phi \end{aligned} \quad (4)$$

We use Eq. 4 to calculate the two-dimensional energy landscape for pairwise capacitively coupled IMT nano-oscillators as shown in Fig. 3(b). The calculated energy landscape exhibits four stable points or attractor states – two degenerate global minima at the out-of-phase configuration and two degenerate local minima at in-phase configuration. By increasing the strength of the capacitive coupling, the attractor states for the out-of-phase configuration becomes more prominent.

A similar investigation is performed for pairwise resistively coupled oscillators as shown schematically in Fig. 3(d). Contrary to the previous case, the measured oscillator phases as well as numerical simulations reveal a higher probability to be in-phase with each other in either $(40^\circ, 40^\circ)$ or $(220^\circ, 220^\circ)$ configuration as shown in Fig. 3(e) for a coupling resistance of $R_C = 40 \text{ k}\Omega$. To establish the nature of resistive coupling, the probability of in-phase configuration is measured as a function of varying R_C and compared to a 2-spin Ising model with ferromagnetic interaction

(positive J). Note that a lower R_C represent a higher coupling strength and hence a higher J . The increase in the probability of in-phase configuration with decreasing R_C , i.e. increasing coupling strength, agrees well with the theoretical Ising model that predicts an increase in probability of parallel configuration ($\uparrow\uparrow, \downarrow\downarrow$) for increasing J as shown in Fig. 3(f). We also use Eq. 4 with $I_{osc,j} = -\frac{V_{osc,j}}{R_{C,j}}$ to calculate the two-dimensional energy landscape as shown in Fig. 3(e), revealing two global and two local energy minima for in-phase and out-of-phase configurations, respectively. This establishes that a ferromagnetic interaction can be replicated using resistive coupling in out PTNO-CTDS based Ising solver. By increasing the strength of the resistive coupling, the attractor states for the in-phase configuration becomes more prominent.

Experimental Demonstration of Max-Cut and Performance Enhancement with Annealing

We investigate the performance of the PTNO-CTDS-based Ising Hamiltonian solver on a NP-hard graph problem of Max-Cut for an undirected and unweighted graph. The Max-Cut problem statement is defined as: Given an undirected graph $G = (V, E)$ with V nodes and E non-negative weights on its edges, the problem requires partitioning G into two subsets W and X such that the total weight on the edges connecting the two subsets is maximized. The Max-Cut problem can be formulated into an equivalent Ising problem using antiferromagnetic interaction ($J = -1$) and we assume the linear Zeeman term to be zero (See Methods section for details). The cut size for a given spin configuration $\vec{\sigma}$ has a direct mapping to the Ising Hamiltonian $H(\vec{\sigma})$, given by $C(\vec{\sigma}) = -\frac{1}{2} \sum_{1 \leq i < j \leq N} J_{ij} - \frac{1}{2} H(\vec{\sigma})$. As such, minimizing the Ising Hamiltonian H maximizes the cut-set C . We chose an undirected and unweighted Mobius Ladder graph with 8 nodes as shown in Fig. 4(a) for our experiment. The phases of the oscillators $\vec{\theta}$ are converted to the Ising spins $\vec{\sigma}$ using discretization windows in the phase space (see Methods section for detail). The PTNOs are connected following the adjacency (or connectivity) matrix of the given graph G using coupling capacitances of equal magnitude. The sinusoidal injection locking signal at twice the oscillator frequency f_0 is applied across the injection capacitances. We implement a linear annealing schedule where the amplitude of the injection locking signal V_{inj} is linearly ramped from zero to a maximum of 10V peak-to-peak over an annealing time T_{anneal} . This is followed by a phase readout time $T_{readout}$. Thus, the total computation time $T_{comp} = T_{anneal} + T_{readout}$. To experimentally investigate to the efficacy of annealing, we vary the annealing time T_{anneal} as shown schematically in Fig. 4(b). For all the cases we keep $T_{readout}$ fixed at 100 oscillation cycles, while T_{anneal} is varied from 0 (representing no anneal scenario) to 660 oscillation cycles.

Fig. 4(c) shows, for a single run, the evolution of the phases of the PTNOs for $T_{anneal} = 3.7$ ms. The equivalent number of oscillations is calculated as $N_{osc} = 250$ cycles. The temporal evolution of the Ising energy and the resultant cut set C is shown in Fig. 4(d) for the case of no anneal and 250 cycle anneal. For the case of no anneal, the application of a high V_{inj} immediately binarizes the phases of the PTNOs. Hence, the corresponding temporal evolution of the Ising energy shows a steep descent. However, as highlighted in Fig. 2(f), the high V_{inj} results in a high dwell time that significantly reduces the temporal fluctuations in the oscillator phases. Thus, with very little freedom to escape the local minima, the network converges to a sub-optimal solution with a higher energy. On the other hand, when we linearly increase V_{inj} over 250 cycles, the dwell time exponentially increases as highlighted in Fig. 2(f) and the temporal fluctuations in the oscillator phases gradually reduce. The network slowly performs energy minimization with more freedom

to escape the local minima and converges to the optimal solution with a higher probability as shown in Fig. 4(d). Thus, we can perform classical annealing in our PTNO-CTDS by controlling the temporal fluctuation in the oscillator phases which is very similar to that of simulated annealing with a decaying noise (or temperature). We also perform numerical simulations using same annealing schemes which show very good agreement with our experimental results.

To quantify the performance of the PTNO-CTDS for varying annealing conditions, we run the network multiple times to calculate the success probability for finding the Max-Cut on this graph instance. The success probability is defined as the ratio of the number of trials that returned the true ground-state energy to the total number of trials. To obtain the true ground-state energy for comparison, we run the same graph instance using the BiqMac solver that executes an exact algorithm (branch-and-bound) on a digital CPU (26) and using a QUBO software called qbsolv (27) developed by D-Wave. Fig. 4(e) shows the success probability increasing with the annealing cycles for both experiments as well as numerical simulations. For example, no anneal scenario resulted in a success probability of 30% obtained experimentally while increasing T_{anneal} to over 600 cycles resulted in a success probability of 96%. These experimental results as well numerical simulations validate our proposed methodology of progressively obtaining better solutions through annealing. The excellent agreement of our numerical simulations with experimental results also enable us to use the simulation framework to predict the performance of the PTNO-CTDS for larger problem size.

Scalability

We start by investigating the performance of the PTNO-CTDS-based Ising solver on a 200 node Mobius Ladder graphs shown in Fig. 5(a). We use a linear anneal scheme over 1,000 cycles. Fig. 5(b) shows the temporal evolution of the oscillator phases governed by the process of energy minimization. Fig. 5(c) shows the increase in the cut size accompanied by a decrease in the equivalent Ising energy as the system evolves towards the ground state configuration. We run the simulation 100 times to calculate a success probability of 95%. Next, we extend the investigation for different problem sizes ranging from 20 to 200 nodes. For each problem size, we consider 20 randomly generated cubic graphs (all nodes have degree 3). Fig. 5(d) shows the ground state energy obtained from our PTNO-CTDS-based Ising solver compared against that calculated by qbsolv (27). The different clusters in the plot represent different problem sizes from 20 to 200 nodes while each data point within a cluster represent 20 randomly generated problems of same size and each problem ran for 100 trials. Fig. 5(d) confirms that our solver is always able to reach the ground state energy for problems up to 200 nodes. However, as anticipated, the distribution of the obtained minimum energy state widens with increasing problem size. This translates to a reduction in the success probability with problem size as shown in Fig. 5(e). We compare simulation results for three different anneal cycles – 100, 500 and 1000. It is seen that, for 200 node problems, the success probability reduces to 1.6% for a short anneal time of 100 cycles. Increasing the anneal time to 500 and 1000 cycles boosts the success probability to 15% and 50%, respectively. Note that, here we report the success probability for obtaining the absolute ground state or the optimum Max-Cut value. Relaxing the solution accuracy to 99% or 95% of the optimum Max-Cut value will incur a much higher success probability. This means that the PTNO-CTDS is capable of finding near-optimal solutions with high probability of success, which has immense implication for tackling real-world industrial problems.

A key metric for benchmarking the performance of any Ising solver is the total computation time required to obtain at least one ground state solution. The total time to solution is calculated directly from Fig. 5(e) as $T_{solution} = T_{comp} [\log(1 - 0.99)] / [\log(1 - P_{success})]$ where the total computation time $T_{comp} = T_{anneal} + T_{readout}$. We assume that, the PTNOs are running at 100MHz in our simulations. With increasing graph size, the success probability of a single run decreases exponentially, necessitating the solver to re-run the problem several times (either serially on the same solver or in a batch mode over multiple solvers) for ensuring a 99% cumulative success probability of obtaining at least one ground state solution. As shown in Fig. 5(f), the total time-to-solution as a function of the graph size N also follows an exponential nature (ae^{bN}) highlighting the NP-hard complexity of the problem. The different time-to-solution curves for different anneal times intersect each other for increasing problem size, thus highlighting a non-trivial dependence of time to solution on the anneal time. Optimizing $T_{solution}$ reveals a tradeoff between the anneal time for a single run and the success probability. It is seen that shorter anneal time of 100 cycles is preferred for small problems up to 50 nodes where the success probability remains very high and is therefore insensitive to the anneal time. However, longer anneal of 100 cycles is preferred for larger problems where the success probability dominates. Thus, the optimum anneal time required increases with the problem size.

We also investigate another key metric for benchmarking the performance - the energy-to-solution for solving such graph problems. For the PTNO-CTDS, the average power consumption for the main compute kernel, i.e. the coupled oscillator network, is estimated to be around $10\mu W$ per oscillator as obtained from circuit simulations (19). We incorporate an additional energy overhead of 20% that will be incurred from the peripheral circuits such as for reading out the phases of the oscillators. The total consumed energy-to-solution is then estimated considering the total time-to-solution from Fig. 5(f). Fig. 5(g) shows the energy-to-solution for increasing problem size and for different anneal schemes. Similar to time-to-solution, we see that shorter anneal times are preferred for small problems where the success probability remains close to unity and is therefore insensitive to the anneal time. However, longer anneal cycles are preferred for larger problems where the success probability dominates.

Performance Comparison with Other Approaches

Table 1 shows the performance of the PTNO-CTDS-based Ising solver compared with other approaches in solving Max-Cut on 100 nodes cubic graphs. We highlight the relevant metrics for comparison such as time-to-solution, energy-to-solution, power dissipated and energy-efficiency (calculated as solutions per second per Watt). For the comparative study, we include five different approaches - (a) well-known simulated annealing algorithm (8) running on an iMac computer with four 3.5 GHz Intel Core i5 processors, (b) a noisy mean-field annealing algorithm running on an NVIDIA GeForce GTX 1080 Ti GPU (28), (c) D-Wave's 2000Q quantum annealer containing 2,048 qubits (16), (d) coherent Ising machine (CIM) based on optical parametric oscillator with an FPGA feedback loop (14, 15) and (e) a discrete-time memristor-based hybrid analog-digital accelerator implementing Hopfield neural network (mem-HNN) (21). Note that mem-HNN belongs to the class of discrete-time dynamical system while ours is a CTDS. On the other hand, CIM is a hybrid electronic-optical accelerator while CPU and GPU are fully digital hardware running heuristic algorithms.

We see a 2x improvement in time-to-solution and 13x lower energy-to-solution for the PTNO-CTDS compared to the discrete-time mem-HNN approach which results in an order of magnitude improvement in energy-efficiency (solution per second per watt). This stems from the fact that the PTNO-CTDS is fully asynchronous and operates in continuous-time while the mem-HNN implementing a Hopfield neural network requires discrete-time updates. We also gain an added benefit in terms of energy dissipation due to the ultra-low power operation of the VO₂-based PTNOs. Compared to D-Wave’s 2000Q quantum annealer, we see a 4x improvement in time-to-solution and over seven orders of magnitude improvement in energy-to-solution. Note that the time-to-solution for D-Wave is highly dependent on the connectivity of the graph and can go up to 10⁴s for dense 100 node graphs with 50% connectivity (16). We do not see such strong dependence of the performance of our PTNO-CTDS-based Ising solver on the sparsity of the graph (23). The huge energy penalty for D-Wave comes from their cryogenic cooling need that requires around 25kW of power. We expect this overhead from cooling to be constant with scaling up to thousands of nodes. The coherent Ising machine (CIM) based on degenerate optical parametric oscillator (DOPO) requires kilometer long fiber cavity to accommodate the DOPO pulses. This incurs a cavity round trip time of microseconds and puts an upper limit on the time-to-solution. For 100 node cubic graphs, we see a 130x improvement in time-to-solution compared to CIM. Also note that although the DOPOs in CIM operate in continuous-time, it requires discrete-time updates measurement-and-feedback schemes for coupling the spins, requiring a 12-bit analog-to-digital converter (ADC), multiple field-programmable-gate-arrays (FPGAs), and high speed transceivers to connect the FPGAs (15) and is inherently serial. We outperform digital CMOS based CPU in terms of time-to-solution and both CPU and GPU in terms of energy-to-solution by orders of magnitude. For GPU, we see a smaller gain of 4x improvement in time-to-solution since GPU also harnesses parallel computation.

In summary, the demonstrated PTNO-CTDS-based Ising solver outperforms all the contemporary approaches towards solving combinatorial optimization problems including fully digital, quantum and optical techniques. We report the best-in-class energy-efficiency of 3.26×10^7 solutions/sec/Watt exhibiting five orders of magnitude improvement when compared with digital CMOS, quantum and photonic approaches and one order of magnitude improvement over the discrete-time memristor-based Hopfield neural network approach. Such a performance gain can be attributed to (a) inherent advantage provided by the CTDS approach harnessing the power of collective-computing with massive parallelism, (b) low-power dissipation of PTNOs, (c) inherent stochasticity of the PTNOs that allows the system to escape local minima and (d) tunable temporal fluctuation of bi-stable oscillator phases allowing implementation of classical annealing in the hardware and progressive evolution towards a globally optimum solution. While the success probability is dependent on the problem size increases for this specific annealing schedule as seen in Fig. 5(e), further improvement is possible in terms of exploring better annealing methodologies or modifying the energy function to avoid non-solution attractor states that trap the system in local minima (29, 30). Hybrid approaches can also be adopted to improve the quality of solution, such as augmenting the search of an Ising solver in the first phase with other metaheuristic local-neighborhood search algorithms such as Tabu search (31) in the second phase. While the concept of utilizing coupled oscillator-based networks for performing computation such as solving optimization problems have been recently explored (32–34), they involve bulky LC oscillators and ring oscillators with latch-based coupling. In comparison, we demonstrate a compact hardware using capacitively coupled one-transistor and one-resistor (1T-1R) PTNOs which provides marked

area and energy benefit (see Supplementary information section S6 for details). Finally, it is to be noted that, while an all-to-all connected oscillator network may not be practically feasible to map a large-scale real-life problem, various avenues of research are being currently pursued that aim at decomposing large-scale problems into smaller Ising/QUBO problems that are might be tractable with practically achievable oscillator networks (27, 35).

Conclusion

The notion of solving hard optimization problems using the continuous-time dynamics of a physical system reveals new avenues of exploration of dynamical systems for compute applications. There is much enthusiasm in building special purpose machines (or accelerators) for solving graph problems belonging to the NP-hard and NP-complete complexity class as part of a strong push towards a heterogenous compute platform. There is a rapidly growing demand to analyze and uncover hidden relationships between similar or diverse datasets in real-time and service applications such as customer analytics, risk and compliance management, recommendation engines, route optimization, fraud detection, asset allocation and risk management. We are witnessing a resurgence in building dedicated optimization processing units (such as Ising Hamiltonian solvers) that can complement general-purpose CPU and GPU. Specialized hardware or accelerators such as Ising solvers are gaining attraction in real-life as many relevant NP-hard and NP-complete problems can be reformulated into the problem of finding the ground state of an Ising model (4). Here, we showcase that exploiting the vast repertoire of emergent complex dynamics exhibited by CTDS enables us to design special purpose hardware that are most appropriate for solving computationally hard optimization problems belonging to the NP-hard or NP-complete complexity class. We believe that the immense benefit of such a CTDS hardware in terms of operating speed and energy dissipation comes from the inherent capability of the system to perform collective-computing in a distributed and highly parallel fashion.

Methods

Sample preparation

10nm thick Vanadium dioxide (VO_2) is grown on a substrate of (001) TiO_2 substrate using Veeco Gen10 molecular beam epitaxy (MBE) system. The widths of the two terminals are defined by dry etching with CF_4 . The device length is defined by depositing Pd/Au metal contacts using electron beam evaporation. The fabricated VO_2 devices varied in length from 100nm to 1 μm with resulting insulator-to-metal transition threshold voltages ranging from 0.7V to 4V. All our experiments have been performed on device lengths of 1 μm .

Experimental setup

Fig. 1(c) shows the schematic of a VO_2 -based PTNO realized by connecting an n-channel MOSFET (ALD1103) transistor in series with the two-terminal VO_2 device. A V_{DD} of 2V is applied and the amplitude of the relaxation oscillations is $\sim 1.7\text{V}$. A gate voltage $V_{\text{GS}} = 0.9\text{V}$ is applied to the series transistor that set the oscillation frequency $f_0 \approx 100\text{kHz}$. Note that when the PTNOs are capacitively coupled, due to loading effect the frequency gets reduced to around 60 – 70 kHz. A schematic of the full experimental setup for the PTNO-based Ising solver is shown in Fig. 1(d). Eight VO_2 devices placed in the Keithley 4200-SCS probe station were connected using multi-contact probes. The V_{DD} and the analog gate voltages V_{GS} of the 8 series transistors are applied using a multichannel analog voltage card connected to a computer. The injection locking

signal was applied to the 8 oscillators across injection locking capacitances $C_{inj} = 20pF$ using an external voltage generator. C_{inj} was realized using discrete off-chip capacitors connected on a breadboard. The output voltage waveforms of the oscillators were measured using a multichannel digital oscilloscope. The coupling among the oscillators was realized using discrete off-chip coupling capacitances $C_c = 56pF$ connected on the breadboard.

Data-processing

The output voltage waveform of the oscillators was measured using a multichannel digital oscilloscope and subsequently analyzed and processed in MATLAB on a digital computer. The phase of an oscillator is calculated with reference to a reference sinusoidal signal with the same frequency f_0 as the oscillator and half of the injection locking signal. The phase is defined as the time difference the minima point of the discharging phase of the IMT oscillator and the minima of the sinusoidal signal divided by the time period of the oscillator (see Supplementary Figure Fig. S4). The measured oscillator phases θ were converted to Ising spins σ using a discretization window in the phase space such that if $90^\circ < \theta < 270^\circ$, $\sigma = 1$, else $\sigma = 0$. Subsequently, the Ising energy and the cut set are calculated. The final energy state of the oscillator network and the corresponding final cut set is calculated during the readout phase as mentioned earlier. We readout the oscillator phases over 100 oscillation cycles.

Numerical Simulation of PTNO network

The numerical simulations for our PTNO network are based on the dynamical system theory as explained in the Supplementary Information section S1. We use a PPV-based numerical simulation methodology (32). For obtaining the PPV function ξ , we use a SPICE compatible macro-model of the IMT nano-oscillator (36) to quantitatively match the dynamics of the oscillators under injection locking conditions, and perform cycle accurate time domain simulations of the PTNO using the Cadence Spectre circuit simulation framework (37). The details are described in the Supplementary Information section S2. The stochastic differential equations describing the PTNO network was numerically solved using the Euler-Maruyama method. The stochasticity of the PTNO is implemented by adding a Gaussian phase noise twice every oscillation cycle. This replicates the inherent stochasticity in abrupt transition from insulator to metallic phase and vice versa occurring twice in every oscillation cycle. In our simulations, the insulator-to-metal transition voltage V_{IMT} was considered as 0.7V and a $V_{DD} = 1V$ was used in our simulations. The total capacitance between the VO_2 device and ground was assumed to be $C_S = 200fF$, while the metallic and insulating resistance of the device was $2k\Omega$ and $100k\Omega$, respectively. The injection locking capacitance $C_{inj} = 1fF$ was used. The resultant operating frequency of the IMT oscillator in our simulation was $f_0 = 100 MHz$. Note that with the current experimental setup being dominated by large parasitic capacitances, the experimentally measured frequency is in kHz. Upon building integrated PTNOs with on-chip coupling, higher operation frequencies up to 100 MHz or above can be practically achieved (22). The time step of our simulation was fixed at 100 ps used. Each simulation run was performed for various anneal times as mentioned in Fig. 5 of the main text. The simulation was further re-run 100 times to calculate the success probability. We found that the success probability of our Ising solver for finding the Max-Cut is sensitive to parameters like the coupling strength and the stochasticity or noise in the system. As such, we varied the strength of the capacitive coupling and the oscillator jitter to find an optimal coupling value and the oscillator jitter that can maximize the success probability (see supplementary information

section S5 for details). For the rest of the scaling simulations reported in Fig 5, we use an optimized coupling capacitance $C_c = 30fF$ and oscillator jitter of 0.5%.

References

1. E. Ising, Beitrag zur theorie des ferromagnetismus. *Zeitschrift für Phys.* **31**, 253–258 (1925).
2. G. Kochenberger, J. K. Hao, F. Glover, M. Lewis, Z. Lü, H. Wang, Y. Wang, The unconstrained binary quadratic programming problem: A survey. *J. Comb. Optim.* (2014), doi:10.1007/s10878-014-9734-0.
3. F. Barahona, On the computational complexity of ising spin glass models. *J. Phys. A. Math. Gen.* (1982), doi:10.1088/0305-4470/15/10/028.
4. A. Lucas, Ising formulations of many NP problems. *Front. Phys.* (2014), doi:10.3389/fphy.2014.00005.
5. M. X. Goemans, D. P. Williamson, Improved Approximation Algorithms for Maximum Cut and Satisfiability Problems Using Semidefinite Programming. *J. ACM* (1995), doi:10.1145/227683.227684.
6. U. Benlic, J. K. Hao, Breakout local search for the max-cut problem. *Eng. Appl. Artif. Intell.* (2013), doi:10.1016/j.engappai.2012.09.001.
7. N. Metropolis, A. W. Rosenbluth, M. N. Rosenbluth, A. H. Teller, E. Teller, Equation of state calculations by fast computing machines. *J. Chem. Phys.* (1953), doi:10.1063/1.1699114.
8. S. Kirkpatrick, C. D. Gelatt, M. P. Vecchi, Optimization by simulated annealing. *Science (80-)*. (1983), doi:10.1126/science.220.4598.671.
9. M. W. Johnson, M. H. S. Amin, S. Gildert, T. Lanting, F. Hamze, N. Dickson, R. Harris, A. J. Berkley, J. Johansson, P. Bunyk, E. M. Chapple, C. Enderud, J. P. Hilton, K. Karimi, E. Ladizinsky, N. Ladizinsky, T. Oh, I. Perminov, C. Rich, M. C. Thom, E. Tolkacheva, C. J. S. Truncik, S. Uchaikin, J. Wang, B. Wilson, G. Rose, Quantum annealing with manufactured spins. *Nature* (2011), doi:10.1038/nature10012.
10. S. Boixo, T. F. Rønnow, S. V. Isakov, Z. Wang, D. Wecker, D. A. Lidar, J. M. Martinis, M. Troyer, Evidence for quantum annealing with more than one hundred qubits. *Nat. Phys.* (2014), doi:10.1038/nphys2900.
11. S. Tsukamoto, M. Takatsu, S. Matsubara, H. Tamura, An accelerator architecture for combinatorial optimization problems. *Fujitsu Sci. Tech. J.* (2017).
12. M. Yamaoka, C. Yoshimura, M. Hayashi, T. Okuyama, H. Aoki, H. Mizuno, in *Digest of Technical Papers - IEEE International Solid-State Circuits Conference* (2015).
13. T. Takemoto, M. Hayashi, C. Yoshimura, M. Yamaoka, in *Digest of Technical Papers - IEEE International Solid-State Circuits Conference* (2019).
14. P. L. McMahon, A. Marandi, Y. Haribara, R. Hamerly, C. Langrock, S. Tamate, T. Inagaki, H. Takesue, S. Utsunomiya, K. Aihara, R. L. Byer, M. M. Fejer, H. Mabuchi, Y. Yamamoto, A fully programmable 100-spin coherent Ising machine with all-to-all connections. *Science (80-)*. (2016), doi:10.1126/science.aah5178.
15. T. Inagaki, Y. Haribara, K. Igarashi, T. Sonobe, S. Tamate, T. Honjo, A. Marandi, P. L. McMahon, T. Umeki, K. Enbutsu, O. Tadanaga, H. Takenouchi, K. Aihara, K. I. Kawarabayashi, K. Inoue, S. Utsunomiya, H. Takesue, A coherent Ising machine for 2000-node optimization problems. *Science (80-)*. (2016), doi:10.1126/science.aah4243.
16. R. Hamerly, T. Inagaki, P. L. McMahon, D. Venturelli, A. Marandi, T. Onodera, E. Ng, C.

- Langrock, K. Inaba, T. Honjo, K. Enbutsu, T. Umeki, R. Kasahara, S. Utsunomiya, S. Kako, K. I. Kawarabayashi, R. L. Byer, M. M. Fejer, H. Mabuchi, D. Englund, E. Rieffel, H. Takesue, Y. Yamamoto, Experimental investigation of performance differences between coherent Ising machines and a quantum annealer. *Sci. Adv.* (2019), doi:10.1126/sciadv.aau0823.
17. D. R. Chialvo, Emergent complex neural dynamics. *Nat. Phys.* (2010), doi:10.1038/nphys1803.
 18. T. J. Wills, C. Lever, F. Cacucci, N. Burgess, J. O’Keefe, Attractor dynamics in the hippocampal representation of the local environment. *Science* (80-.). (2005), doi:10.1126/science.1108905.
 19. S. Dutta, A. Parihar, A. Khanna, J. Gomez, W. Chakraborty, M. Jerry, B. Grisafe, A. Raychowdhury, S. Datta, Programmable coupled oscillators for synchronized locomotion. *Nat. Commun.* (2019), doi:10.1038/s41467-019-11198-6.
 20. S. H. Strogatz, I. Stewart, Coupled Oscillators and Biological Synchronization. *Sci. Am.* **269**, 102–109 (1993).
 21. F. Cai, S. Kumar, T. Van Vaerenbergh, X. Sheng, R. Liu, C. Li, Z. Liu, M. Foltin, S. Yu, Q. Xia, J. J. Yang, R. Beausoleil, W. D. Lu, J. P. Strachan, Power-efficient combinatorial optimization using intrinsic noise in memristor Hopfield neural networks. *Nat. Electron.* (2020), doi:10.1038/s41928-020-0436-6.
 22. N. Shukla, A. Parihar, E. Freeman, H. Paik, G. Stone, V. Narayanan, H. Wen, Z. Cai, V. Gopalan, R. Engel-Herbert, D. G. Schlom, A. Raychowdhury, S. Datta, Synchronized charge oscillations in correlated electron systems. *Sci. Rep.* **4**, 1–6 (2014).
 23. S. Dutta, A. Khanna, J. Gomez, K. Ni, Z. Toroczkai, S. Datta, (IEEE International Electron Devices Meeting (IEDM), 2019).
 24. S. Dutta, A. Khanna, W. Chakraborty, J. Gomez, S. Joshi, S. Datta, in *2019 Symposium on VLSI Technology* (IEEE, 2019), pp. T128–T129.
 25. A. Parihar, M. Jerry, S. Datta, A. Raychowdhury, Stochastic IMT (Insulator-metal-transition) Neurons: An interplay of thermal and threshold noise at bifurcation. *Front. Neurosci.* **12**, 1–8 (2018).
 26. A. Wiegele, Biq Mac Library—A collection of Max-Cut and quadratic 0-1 programming instances of medium size. *Preprint* (2007).
 27. M. Booth, S. P. Reinhardt, A. Roy, Partitioning optimization problems for hybrid classical. *quantum Exec. Tech. Rep.*, 1–9 (2017).
 28. A. D. King, W. Bernoudy, J. King, A. J. Berkley, T. Lanting, Emulating the coherent Ising machine with a mean-field algorithm. *arXiv Prepr. arXiv1806.08422* (2018).
 29. M. Ercsey-Ravasz, Z. Toroczkai, Optimization hardness as transient chaos in an analog approach to constraint satisfaction. *Nat. Phys.* (2011), doi:10.1038/NPHYS2105.
 30. B. Molnár, F. Molnár, M. Varga, Z. Toroczkai, M. Ercsey-Ravasz, A continuous-time MaxSAT solver with high analog performance. *Nat. Commun.* (2018), doi:10.1038/s41467-018-07327-2.
 31. F. Glover, Future paths for integer programming and links to artificial intelligence. *Comput. Oper. Res.* (1986), doi:10.1016/0305-0548(86)90048-1.
 32. T. Wang, J. Roychowdhury, in *Lecture Notes in Computer Science (including subseries Lecture Notes in Artificial Intelligence and Lecture Notes in Bioinformatics)* (2019).
 33. J. Chou, S. Bramhavar, S. Ghosh, W. Herzog, Analog Coupled Oscillator Based Weighted Ising Machine. *Sci. Rep.* (2019), doi:10.1038/s41598-019-49699-5.

34. I. Ahmed, P.-W. Chiu, C. H. Kim, in *Symposia on VLSI Technology and Circuits* (2020).
35. F. Neukart, G. Compostella, C. Seidel, D. von Dollen, S. Yarkoni, B. Parney, Traffic flow optimization using a quantum annealer. *Front. ICT* (2017), doi:10.3389/fict.2017.00029.
36. P. Maffezzoni, L. Daniel, N. Shukla, S. Datta, A. Raychowdhury, Modeling and Simulation of Vanadium Dioxide Relaxation Oscillators. *IEEE Trans. Circuits Syst. I Regul. Pap.* **62**, 2207–2215 (2015).
37. V. S. C. Simulator, Cadence Design Systems. *Inc.*, Available www.cadence.com (2005).

Author contributions

S. Dutta and S. Datta conceived the idea. S. Dutta and A.K. performed the measurements, analyzed the data and performed simulations. A.K. fabricated the devices. H.P. and D.S. did MBE growth of the VO₂ samples. A.R. and Z.T. participated in useful discussions. S. Dutta, A.K., A.R., Z.T. and S. Datta participated in the writing of the manuscript.

Competing interests

The authors declare no competing interests.

Figure 1

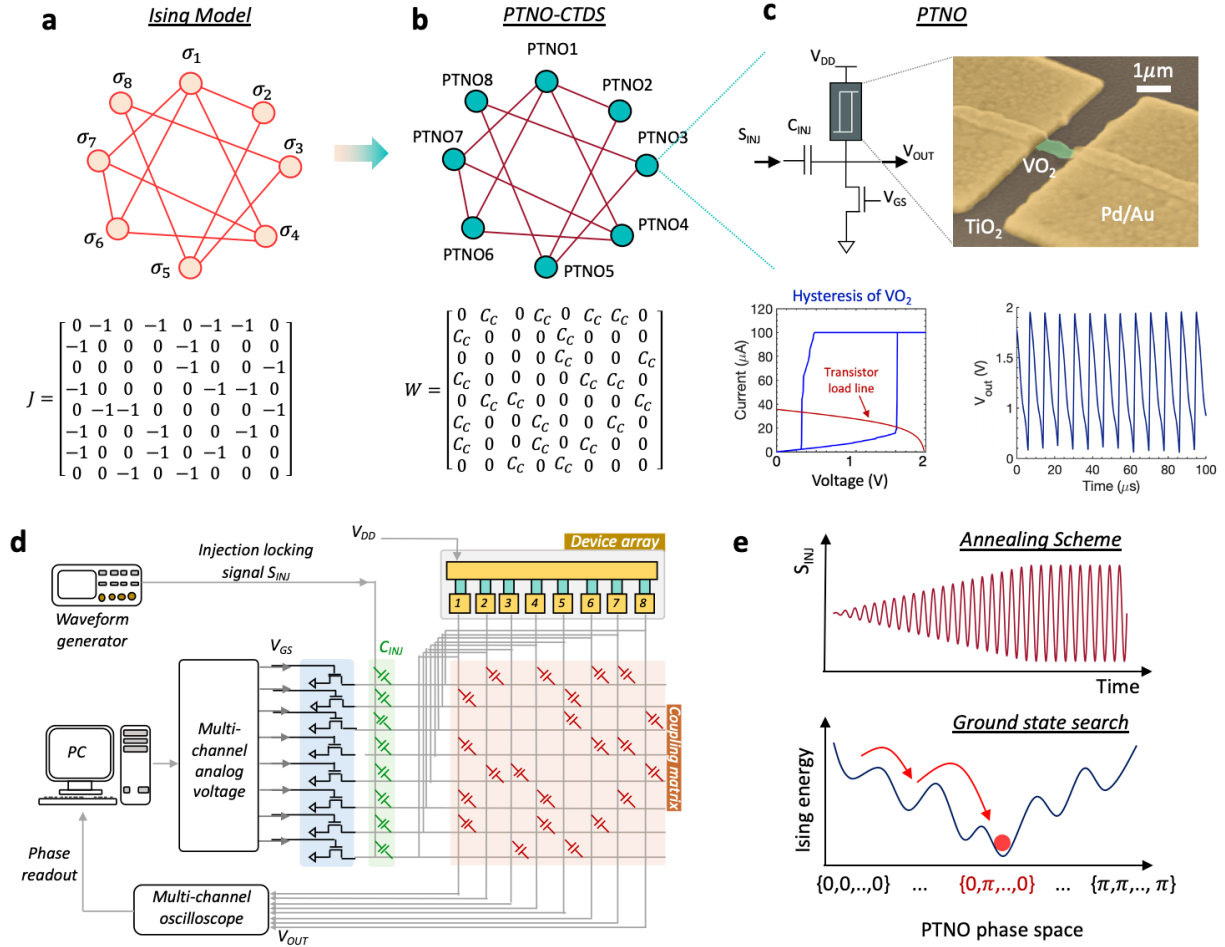


Fig. 1. Overview of PTNO-based CTDS as an Ising Hamiltonian solver. (a, b) The combinatorial optimization problem is reformulated in terms of the Ising Hamiltonian H defined by the spin vector $\vec{\sigma}$, and the symmetric coupling matrix J and mapped onto the Ising solver. Each Ising spin, representing a node in the graph is represented by an insulator-to-metal (IMT) phase-transition nano-oscillator (PTNO). The PTNOs are coupled to each other using passive elements such as capacitances. The coupling matrix W for the PTNO network is derived from the adjacency or coupling matrix J of the Ising model. (c) Schematic of a PTNO consisting of a two-terminal phase-transition hysteretic device (VO_2) in series with a transistor. As the load line of the series transistor passes through the unstable hysteresis region of the VO_2 device, self-sustained oscillations are created. (d) Experimental setup of our PTNO-based CTDS. The main computing kernel comprises eight PTNOs connected using coupling capacitance following the coupling matrix W . The phenomenon of second harmonic injection locking (SHIL) is used to create bistable oscillator phases, emulating artificial Ising spin. (e) The inherent stochasticity present in the PTNO along with a novel technique of gradually reducing the temporal fluctuations in the oscillator phases by increasing the strength of the injection locking signal S_{INJ} is utilized to perform classical annealing and obtain progressively better solutions.

Figure 2

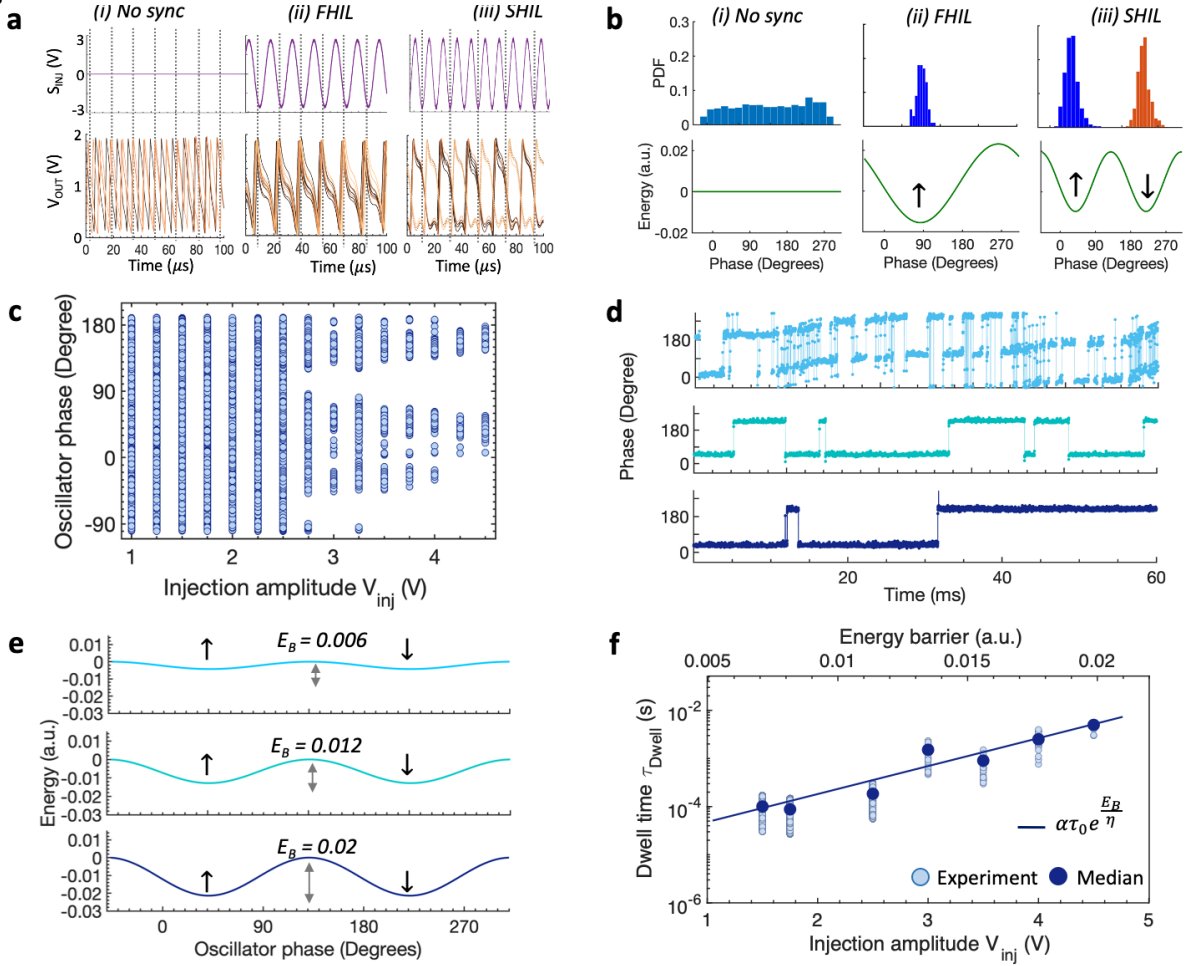


Fig. 2. Creating artificial Ising spin using second harmonic injection locking (SHIL). (a) Three different injection locking scenarios are shown. No synchronization case refers to free running oscillator with uniform of oscillator phase in the phase space. For first harmonic synchronization (FHIL), the oscillator remains injection locked with input signal at in-phase configuration. For second harmonic synchronization (SHIL), the oscillator phase gets binarized into in-phase and out-of-phase configuration with equal probability. (b) Measured distribution of the oscillator phases for the three scenarios along with the equivalent Ising energy for a single PTNO is shown depicting zero, one and two energy minima for stable phase locking, respectively. (c) Increasing the amplitude (V_{inj}) of SHIL forces the oscillator into bi-stable phase configuration. (d) The increase in V_{inj} also reduces the temporal fluctuations between the two stable phases in the presence of noise. (e) Modulation of the energy landscape with V_{inj} . The three curves correspond to $V_{inj} = 1V, 3V$ and $5V$. Increasing V_{inj} increases the energy barrier between the two bi-stable energy minima states. This tightens the phase distribution as seen in (c). (f) The mean dwell time (τ_{Dwell}) spent by an oscillator before hopping between the two phases is plotted against the applied injection locking amplitude and is found to follow a Arrhenius type law ($\alpha\tau_0 e^{E_B/\eta}$) with the inherent stochasticity (η) playing the role of temperature. $\tau_0 = \frac{1}{f_0}$ is the characteristic or attempt time (equal to the time period of the oscillator) and α is the fitting parameter.

Figure 3

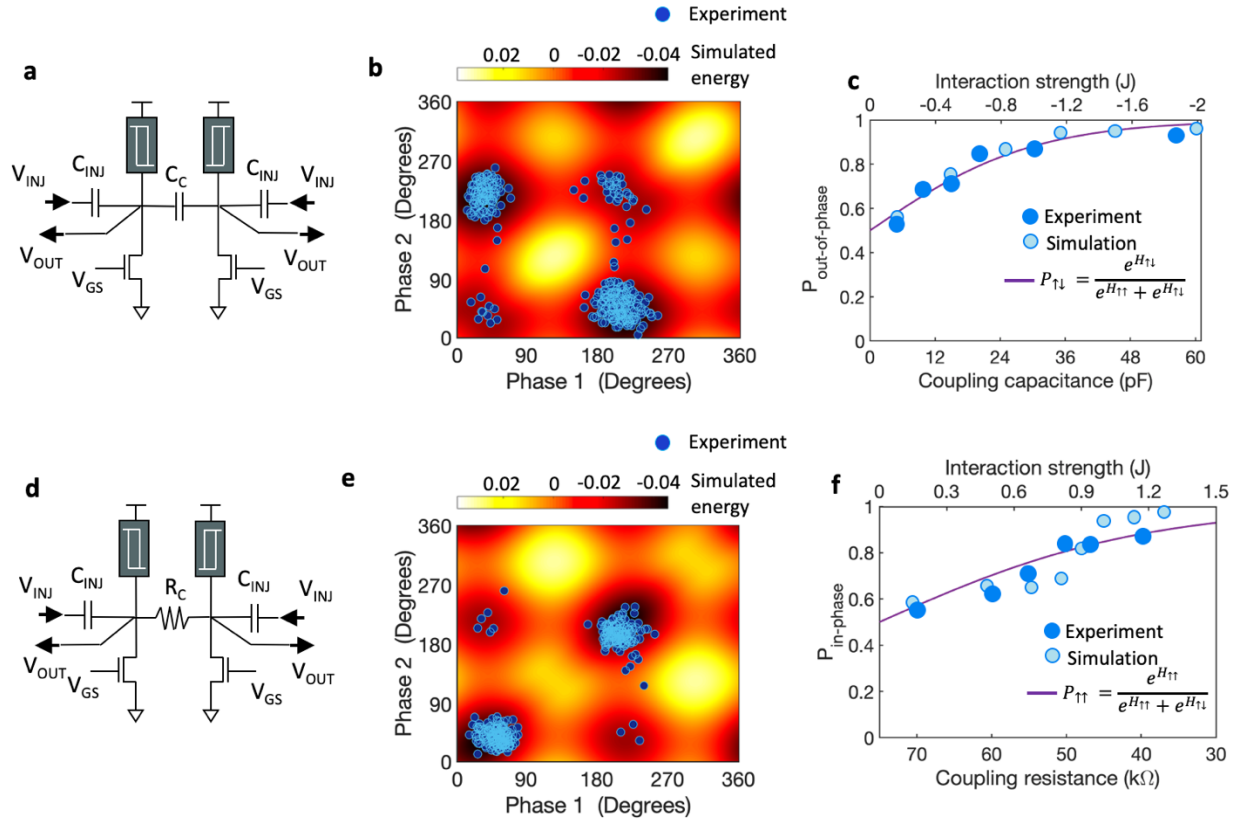


Fig. 3. Replicating ferromagnetic and anti-ferromagnetic Ising interactions. (a) Schematic of pairwise capacitively coupled PTNOs. (b) Measured distribution of the phases of the two PTNOs, highlighting the preference of the oscillators to remain in a stable out-of-phase configuration. The calculated energy landscape for capacitive coupling also highlights the presence of global energy minima corresponding to the out-of-phase configuration. (c) The measured probability of out-of-phase configuration as a function of varying capacitive coupling strength establishes the equivalent anti-ferromagnetic nature of interaction when compared to a 2-spin Ising model. (d) Schematic of pairwise resistively coupled PTNOs. (e) The measured phase distribution for resistive coupling along with the calculated energy landscape showing the preference for in-phase configuration. (f) The measured probability of in-phase configuration vs coupling strength highlights the ferromagnetic nature of interaction for resistively coupled oscillators.

Figure 4

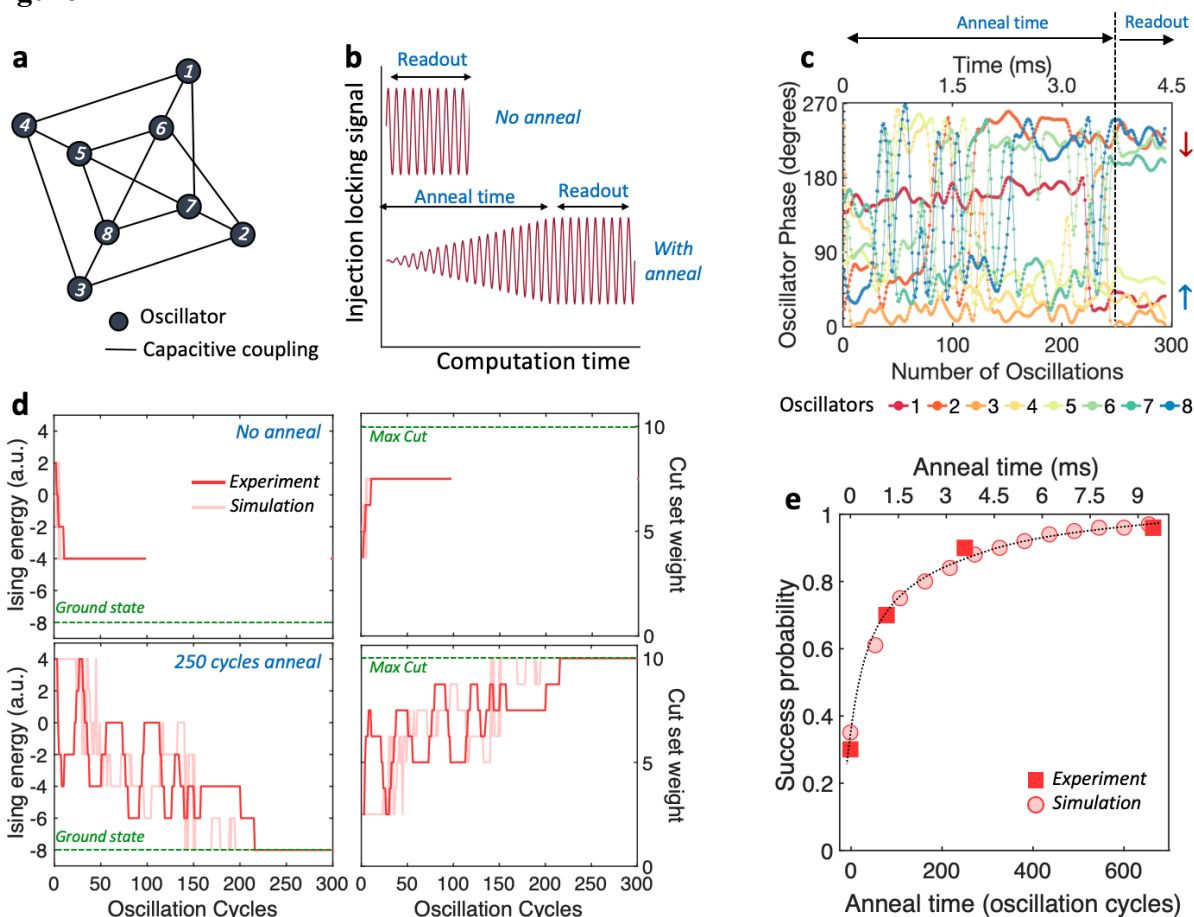


Fig. 4. Experimental demonstration of Max-Cut and performance enhancement with annealing. (a) An undirected and unweighted 8-node Mobius Ladder graph used for investigating the Max-Cut. The PTNOs are connected following the same adjacency (or connectivity) matrix of the graph using coupling capacitances. (b) Schematic of the annealing schedule used in the experiment. A sinusoidal injection locking signal at twice the oscillator frequency f_0 is applied with a linearly increasing amplitude over the annealing time T_{anneal} that corresponds to a linear annealing schedule. This is followed by a phase readout time $T_{readout}$. Thus, the total computation time $T_{comp} = T_{anneal} + T_{readout}$. The annealing time T_{anneal} is varied from zero (corresponding to no anneal) to 660 oscillation cycles. (c) Evolution of the phases of the 8 oscillators, settling to either in-phase or out-of-phase with the injection locking signal. (d) The calculated temporal evolution of the Ising Hamiltonian shows an energy minimization accompanied by an increase in the graph cut size. For no annealing scheme, the network converges to a sub-optimal solution with a higher energy while annealing over 250 cycles allows the network to converge to the optimal solution with a lower Ising energy with a higher probability. Numerical simulations using same annealing schemes show very good agreement with our experimental results. (e) Experimental data and numerical simulation results for the success probability for different anneal times showing a steady increase from 30% with no anneal to 96% for over 600 cycles of linear anneal.

Figure 5

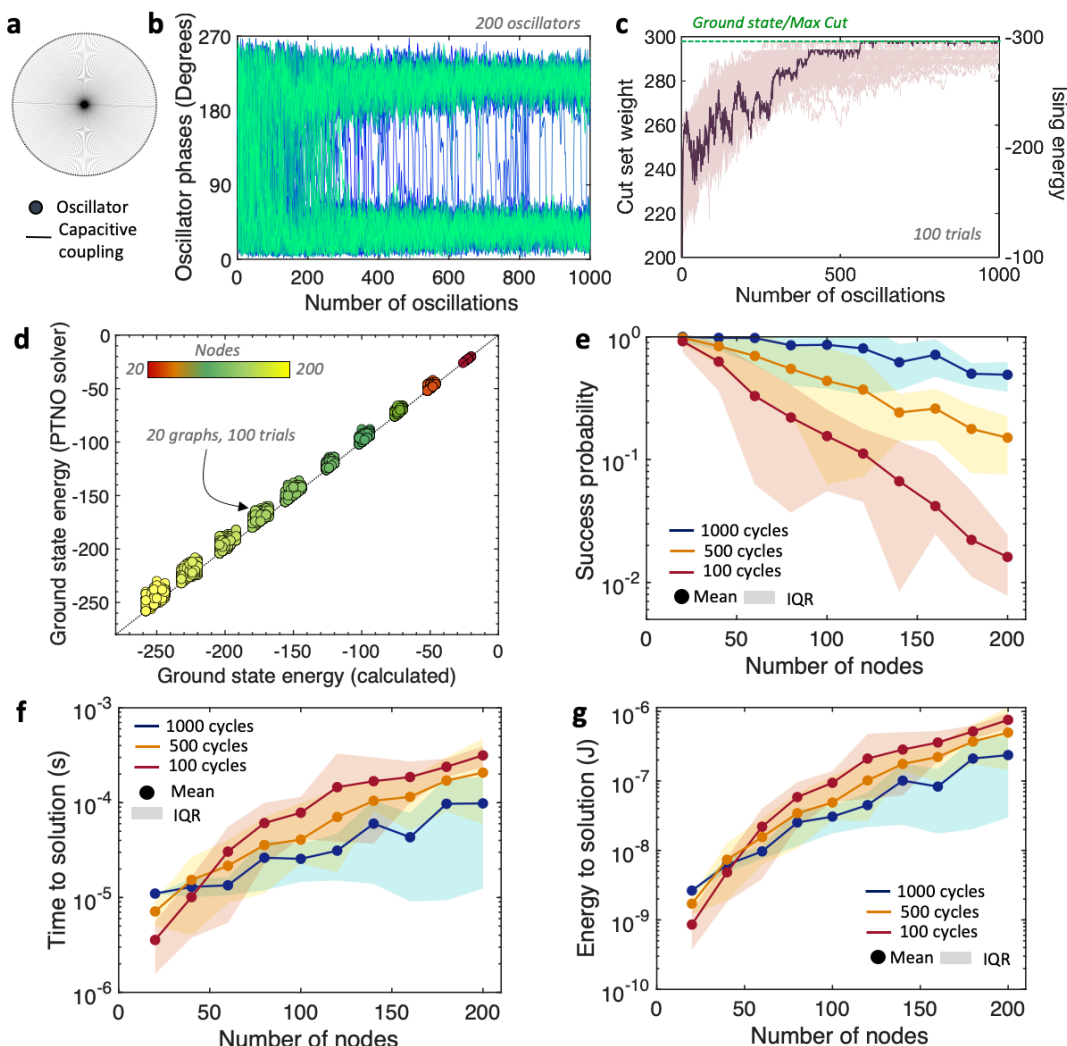


Fig. 5. Performance of PTNO-CTDs-based Ising Hamiltonian solver and scaling with problem size. (a) Schematic of a 200 node Mobius ladder graph used for numerical simulation. **(b)** The evolution of the phases of the oscillators for a single run as a function of oscillation cycles. **(c)** Increase in the graph cut size accompanied by a decrease in the equivalent Ising energy as the system evolves towards the ground state configuration. The simulation was performed for 100 trials to calculate a success probability of 95%. **(d)** Comparison between the ground state energy obtained from our PTNO-CTDS-based Ising solver and that calculated by qbsolv (27) for randomly generated cubic graphs (all nodes have degree 3). Different clusters represent different problem sizes ranging from 20 to 200 nodes while each data point within a cluster represent 20 randomly generated problems of same size and each problem ran for 100 trials. **(e)** Success probability of finding the ground state for random cubic graphs of varying size. We compare simulation results for three different anneal cycles – 100, 500 and 1000. **(f)** The total time-to-solution for different anneal times and for varying problem size. A non-trivial dependence of time to solution on the anneal time is seen where shorter anneal time is preferred for smaller problems where the success probability remains insensitive to the anneal time. Longer anneal is preferred for larger problems where the success probability dominates. **(g)** Energy-to-solution plotted for different anneal times and for varying problem size showing a similar trade-off is seen.

Table 1. Performance comparison between PTNO-CTDS-based Ising solver and other state-of-the-art approaches. Comparison done for solving Max-Cut on 100 nodes random cubic graphs.

	Simulated Annealing (CPU)	Noisy mean-field annealing (GPU)	D-Wave 2000Q	Coherent Ising Machine (CIM)	Memristor-based Hopfield network (mem-HNN)	Phase Transition Nano-oscillator (PTNO)
Represent spins	Spins	Spins	Qubits	Coherent light	-	Oscillator phases
Interaction	Ising interaction	Ising interaction	Flux storage	FPGA	-	Capacitance/Resistance
Update mechanism	Synchronous	Synchronous	Synchronous	Asynchronous	Hybrid [#]	Asynchronous
Connectivity	All-to-all	All-to-all	Sparse	All-to-all	All-to-all	All-to-all
Annealing scheme	Classical annealing	Classical annealing	Quantum annealing	Coherent computing	Modulate intrinsic noise	Classical annealing
Scaling with problem	e^{-N}	e^{-N}	e^{-N^2}	e^{-N}	e^{-N}	e^{-N}
Cryogenic cooling	No	No	Yes	No	No	No
Time to solution	246ms	100 μ s	100 μ s	3.3ms	40 μ s*	25.5 μ s
Energy to solution	14.8J	< 25mJ	2.5J	-	0.4 μ J	30.6nJ
Power	60W [§]	< 250W	25kW	-	10.9mW	1.2mW
Energy efficiency (Solutions/sec/W att)	6.7x10 ⁻²	> 40	0.4	-	2.5x10 ⁶	3.26x10 ⁷

[§] SA algorithm implemented on a CPU using 4 Intel Core i5 processors each running at 3.5GHz

[#]Hybrid scheme updates 10 nodes at a time

*Reported for 300 cycles performed sequentially.